A Novel Bismuth-Based Metal-Organic Framework for High Volumetric Methane and Carbon Dioxide Adsorption

Mathew Savage,[1] Sihai Yang,[1] Mikhail Suyetin,[1] Elena Bichoutskaia,[1] Alexander J. Blake,[1] Sarah A. Barnett[2] and Martin Schröder[1]*

1. School of Chemistry, University of Nottingham, University Park, Nottingham NG7 2RD, UK. Fax: +44 115 9513563; Tel: +44 115 9513490; E-mail: M.Schroder@nottingham.ac.uk.
2. Diamond Light Source, Harwell Science and Innovation Campus, Didcot, Oxfordshire, OX11 0DE, UK

Keywords

Bismuth, metal-organic framework, carboxylate, methane, CO_2, grand canonical Monte Carlo simulations

Abstract

Solvothermal reaction of H_4L (L = biphenyl-3,3',5,5'-tetracarboxylate) and $Bi(NO_3)_3 \cdot (H_2O)_5$ in a mixture of DMF/MeCN/H_2O in the presence of piperazine and nitric acid at 100 ^oC for 10 h affords the solvated metal-organic polymer $[Bi_2(L)_{1.5}(H_2O)_2] \cdot (DMF)_{3.5} \cdot (H_2O)_3$ (NOTT-220-solv). A single crystal X-ray structure determination confirms that it crystallises in space group *P*2/*c* and has a neutral and non-interpenetrated structure comprising binuclear $\{Bi_2\}$ centres bridged by tetracarboxylate ligands. NOTT-220-solv shows a 3,6-connected network having a new framework topology with a $\{4 \cdot 6^2\}_2\{4^2 \cdot 6^5 \cdot 8^8\}\{6^2 \cdot 8\}$ point symbol. The desolvated material NOTT-220a shows exceptionally high adsorption uptakes for CH_4 and CO_2 on a volumetric basis at moderate pressures and temperatures with a CO_2 uptake of 553 gL^{-1} (20 bar, 293 K) with a saturation uptake of 688 gL^{-1} (1 bar, 195 K). The corresponding CH_4 uptake of 165 V(STP)/V (20 bar, 293 K) and 189 V(STP/V) (35 bar, 293 K) is within the top three MOF materials under the same conditions, surpassed only by PCN-14 and Ni-MOF-74 (230 and 190 V(STP)/V 35 Bar, 298 K). The maximum CH_4 uptake for NOTT-220a was recorded at 20 bar and 195 K to be 287 V(STP)/V, while H_2 uptake of NOTT-220a at 20 bar, 77 K is 42 gL^{-1}. These gas uptakes have been modelled by Grand Canonical Monte Carlo (GCMC) and Density Functional Theory (DFT) calculations, which confirm the experimental data and give insights into the nature of the binding sites of CH_4 and CO_2 in this porous hybrid material.

Introduction

Porous metal-organic frameworks (MOFs) have attracted major research interest due to their potential in a wide range of applications, in particular in the field of gas adsorption and separation.[1] This research is of importance not only for the development of energy storage media for hydrogen (H_2) or methane (CH_4),[2] but also for the design of new carbon capture systems.[3] MOF materials exhibit three-dimensional extended structures incorporating both large accessible pore volume and high internal surface area, which are key features for high capacity gas adsorption. They are often based upon divalent late first row transition metals [*eg.* Cu(II) and Zn(II)] and polycarboxylate ligands, and can show low framework densities (0.22-0.9 g cm^{-3}) leading to high gravimetric gas uptakes.[4] Thus, a great deal of current effort is focused on the synthesis of low density MOFs by using elongated organic ligands[4a-c] and/or light metal ions (*e.g.* Li,[5] Be,[6] Mg[7]), in order to maximise and enhance gravimetric gas uptakes.

Despite intense research on H_2 storage materials in recent years, no feasible storage media have been discovered to meet DoE storage capacity targets at moderate temperature and pressure.[8] Thus, as a promising alternative to H_2, CH_4 is attracting considerable interest for on-board mobile applications due to its high molar energy density and low carbon content, leading to lower carbon dioxide (CO_2) emissions by combustion.[2] However, at ambient temperatures and pressures, CH_4 has a low energy density in the gaseous phase, but this density can be increased by compression or liquefaction. Compressed natural gas requires bulky, heavy-walled storage tanks and expensive dual-stage compressors, while liquefaction of methane can only be achieved at cryogenic temperatures, necessitating complex tank design in order to maintain the low temperature and reduce boil-off. As a result, neither of these approaches is suitable for light-duty and small consumer automobiles.

The alternative is to use porous sorbents to store natural gas at high density at ambient temperatures and moderate pressures (typically 35 bar). Volumetric gas uptake is an important criterion if these systems are to find practical applications, because high volumetric uptake minimises the volume of storage material and therefore the size of the fuel tank. This is of critical importance as it will allow adsorbed natural gas tanks to be more optimally integrated into the limited space available within a small vehicle. Unfortunately, low-density MOFs, even those with high gravimetric gas uptake, typically have low volumetric uptakes as a consequence of their low density. Moreover, very low density MOFs with high percentage pore voids often show poor framework stability upon removal of guest solvents, resulting in the decomposition of the

material.[9] We report herein the development of a unique highly porous and high-density porous system NOTT-220-solv constructed from biphenyl-3,3',5,5'-tetracarboxylate (L^{4-}) (Scheme 1) and Bi^{3+} ions, a metal which is rarely used in MOF construction due partly to its high density.[10] NOTT-220-solv shows a new framework topology based upon binuclear {Bi_2} nodes, and the combination of a large pore void (up to 54%) and a high bulk density (1.46 g cm^{-3}) leads to exceptionally high volumetric gas uptakes in desolvated NOTT-220a at saturation: 287 V(STP)/V for CH_4 at 195 K, 20 bar; 688 gL^{-1} for CO_2 at 195 K, 1.0 bar. The experimental uptakes for CH_4 have been confirmed by modelling studies and confirm that at ambient temperatures the volumetric CH_4 uptake in NOTT-220a [189 V(STP/V) at 35 bar and 293 K] equals that observed for Ni-MOF-74,[11] and exceeds all other porous MOF systems reported to date under the same conditions apart from PCN-14 [230 V(STP)/V at 35 bar and 290 K].[12]

Experimental

Synthesis of NOTT-220-solv

H_4L (Scheme 1) (15 mg, 0.045 mmol), $Bi(NO_3)_3 \cdot (H_2O)_5$ (17 mg, 0.035 mmol) and piperazine (7.0 mg, 0.081 mmol) were combined in a 23 mL glass pressure tube. DMF/MeCN mixture (1.3 ml, 1:0.3 v/v) was added to the tube and the white slurry was acidified with dilute nitric acid (5 %, 0.3 mL). The reaction vessel was heated to 100°C in an oil bath for 10 hours. When a white crystalline precipitate was observed, the hot reaction vessel was quickly cooled with cold water to avoid the formation of recrystallised ligand as impurities. The white crystalline powder was washed sequentially with DMF, and dried briefly in air. Yield: 10 mg (25 %). Elemental anaylsis (% calc/found): $[Bi_2(C_{16}H_6O_6)_{1.5}(H_2O)_2] \cdot (DMF)_{3.5} \cdot (H_2O)_3$ (C 34.5/34.0, H 3.6/3.1, N 3.5/4.1). The volatility of crystallisation solvents in the samples contributes to the discrepancy in elemental analytical data. Selected IR(ATR): ν/cm^{-1} = 3366 (b) H_2O, 2928 (w) C-H, 2160 (w), 1978 (w), 1645 (s) O-H, 1539 (m) C-O, 1315 (m), 1252 (m) C-O, 1097 (m), 906 (w), 851 (w), 770 (m), 735 (s), 661 (s).

Gas adsorption isotherms

H_2, N_2, CO_2 and CH_4 isotherms (0-20 bar) were recorded at 77 K (by liquid nitrogen) or 87 K (by liquid argon) or 273 and 293 K (by temperature-programmed water bath) on an IGA-003 system (Hiden Isochema, Warrington, UK) at the University of Nottingham under ultra high vacuum in a clean system with a diaphragm and turbo pumping system. Ultra-pure plus grade (99.9995%) H_2 was purchased from BOC and

purified further using calcium aluminosilicate and activated carbon adsorbents to remove trace amounts of water and other impurities before introduction into the IGA system, Research grade CH_4, CO_2 and N_2 were purchased from BOC and used as received. Powder samples were loaded into the IGA and degassed at 100 °C and 10^{-10} bar for 1 day to give desolvated samples. In a typical procedure, ~50 mg of dry sample was used for the measurements.

X-ray crystallography

X-ray diffraction data on single crystals of NOTT-220-solv were collected at 100(2) K on a Bruker APEXII CCD area detector using graphite monochromated Mo-*K*α radiation from a rotating anode source at the UK National Crystallography Service and at 120(2) K on a Rigaku Saturn 724+ detector using silicon double-crystal monochromated synchrotron radiation of wavelength 0.6889 Å on Beamline I19 at Diamond Light Source. Structures were solved by direct methods and developed by difference Fourier techniques using the SHELXTL[13] software package. The hydrogen atoms on the ligands were placed geometrically and refined using a riding model. The hydrogen atoms of coordinated water molecules could not be located but are included in the molecular formula and in values derived from it. The unit cell volume includes a large region of disordered solvent, which could not be modelled as discrete atomic sites. We employed PLATON/SQUEEZE[14] to calculate the contribution to the diffraction from the solvent region and thereby produced a set of solvent-free diffraction intensities. The final formula was calculated from elemental analysis data combined with TGA analysis: the contents of the solvent region are therefore included in the unit cell contents but not in the refinement model.

Crystal data for *α*-NOTT-220-solv. $[Bi_4(C_{16}H_6O_6)_3(H_2O)_4]\cdot(DMF)_7\cdot(H_2O)_6$. Colourless chip (0.03 x 0.02 x 0.01 mm). *P*2/*c*, a = 19.567(6), b = 9.869(3), c = 22.135(6) Å, β = 104.81(1) °, V = 4132(2) Å^3, Z = 2, D_{calc} = 2.014 g cm^{-3}, μ = 8.591 mm^{-1}, F(000) = 2420. A total of 18307 reflections was collected, of which 9298 were unique giving R_{int} = 0.107. Final R_1 (wR_2) = 0.0745 (0.185) with GOF = 0.80. The final difference Fourier extrema were 3.94 and -3.16 e/Å^3. CCDC repository number 899427.

Crystal data for *β*-NOTT-220-solv. $[Bi_4(C_{16}H_6O_6)_3(H_2O)_4]\cdot(DMF)_7\cdot(H_2O)_6$. Colourless chip (0.03 x 0.02 x 0.01 mm). *P*2/*c*, a = 19.721(10), b = 9.862(5), c = 22.179(11) Å, β =105.35(1) °, V = 4160(4) Å^3, Z = 2, D_{calc} = 2.001 g cm^{-3}, μ = 8.535 mm^{-1}, F(000) = 2420. A total of 26446 reflections was collected, of which 7290 were unique, giving R_{int} = 0.119. Final R_1 (wR_2) = 0.0934 (0.273) with GOF = 1.04. The final difference Fourier extrema were 5.23 and -3.21 e/Å^3. CCDC repository number 899428.

Modelling and simulations

Grand Canonical Monte Carlo (GCMC) simulations were performed using the MUSIC simulation suite[15] to calculate the adsorption of CH_4 and CO_2 molecules in NOTT-220a. The GCMC simulations involved $1.25 \cdot 10^7$ steps equilibration period followed by $1.25 \cdot 10^7$ steps production run for the methane uptake simulation, and $2 \cdot 10^7$ steps equilibration period followed by $2 \cdot 10^7$ steps production run for the CO_2 uptake simulation. The CH_4 molecule was described using a set of united-atom Lennard-Jones interaction parameters, σ_O=3.73 Å, ε_O/k_B = 148.0 K, obtained from fitting to critical temperatures and saturated liquid densities.[16] The CO_2 molecule was described using a force field which quantitatively reproduces the vapour-liquid equilibrium (VLE) of the neat system and the binary mixtures. All three atoms of the CO_2 molecule were described as a set of united-atom Lennard-Jones interaction sites and described with the following parameters: σ_O=3.05 Å, ε_O/k_B = 79 K for oxygen atoms, and σ_C = 2.80 Å, ε_C/k_B = 27 K for the carbon atom. A point charge of +0.7 was placed at the centre of mass of carbon atom and a point charge of −0.35 was placed at each oxygen atom, the C−O bond length taken to be 1.16 Å. All atoms in the MOF structure were described by an OPLS force field[17] with the exception of Bi atom, which was described by universal force field parameters[18] and oxygen atoms, for which the force-field parameters were taken from a literature value.[19] The simulation supercell contained six (2x1x3) unit cells with periodic boundary conditions. The fugacity has been calculated from the Peng-Robinson equation of state[20] and the MOF and the guest gas molecules were considered to be rigid. A Lennard-Jones potential has been used to describe the Van der Waals interactions with a cut-off distance of 14.0 Å.

Density Functional Theory (DFT) calculations were performed to derive the partial atomic charges subsequently used in the GCMC calculations and to calculate the binding energy of CH_4 and CO_2 to the binuclear Bi node. The DFT calculations were performed with the Q-Chem quantum chemistry package[21] using the B3LYP level of theory and the 6-31G* basis set, partial atomic charges were obtained using the ChelpG technique.[22] To determine the binding energy geometry optimisations were performed at the B3LYP/6-31G** level of theory, and the binding energies were subsequently calculated at the higher B3LYP /6-311++G** level as follows BE = E(complex) - E(linker) - $E_{opt}(CH_4)$.

Results and Discussion

Solvothermal reaction of H_4L (Scheme 1) and $Bi(NO_3)_3 \cdot (H_2O)_5$ in a mixture of DMF/MeCN in the presence of piperazine and nitric acid at 100 ^oC for 10 h affords the solvated material NOTT-220-solv. In our hands, the addition of both piperazine and nitric acid in the synthesis are essential for the formation of NOTT-220-solv. In the absence of piperazine or nitric acid, NOTT-220-solv cannot be obtained or is formed together within an intractable mixture with other products. Single crystal diffraction data of NOTT-220-solv confirms that it crystallises in space group *P*2/*c* and has a neutral and non-interpenetrated structure constructed from binuclear $\{Bi_2\}$ centres bridged by tetracarboxylate ligands. Interestingly, the Bi(III) centres in two solved crystal structures (denoted as *alpha* and *beta* phases) have slightly altered coordination environments (Scheme 2). In both phases, each Bi(III) ion is coordinated to three carboxylate groups from three different L^{4-} ligands [Bi—O = 2.280(12)-2.579(10) Å], and both Bi(III) ions share three oxygen atoms from three bridging carboxylate groups [Bi—O = 2.481(10)-2.691(11) Å] to give irregular distorted pseudo-tetrahedral $[Bi_2(O_2CR)_6]$ nodes (Scheme 2). In addition, each node is coordinated to two water molecules. In the *alpha* phase, one water molecule resides on each Bi(III) ion [Bi1—O13 = 2.582(12) Å, Bi2—O14 = 2.517(13) Å] to give a coordination number of 8 for Bi1 and 9 for Bi2. In the *beta* phase, both water molecules reside on the same Bi(III) ion, resulting in coordination numbers of 9 for Bi1 and 8 for Bi2 [Bi1—O13 = 2.659(12) Å, Bi1—O14 = 2.696(11) Å]. Pairs of ligands at opposite sides of the node participate in an offset face to face π-π stacking interaction [perpendicular distance: 3.494(9) Å]. If the $\{Bi_2\}$ node is considered as a singular 6-c vertex, and the ligand as two 3-c vertices, an overall 3,6-connected framework structure is formed with a new topology with a point symbol of $\{4\cdot6^2\}_2\{4^2\cdot6^5\cdot8^8\}\{6^2\cdot8\}$ according to the TOPOS database[23] (Figure 1). However, if the pair of π-stacked ligands is considered as one ligand, the topology of the structure simplifies to the **tfi** topology, with a point symbol of $\{6^2,8^4\}\{6^2,8\}$ (Figure S3).

Due to the overall extended structure, the unit cell, the space group and symmetry of the two phases of the material are identical and differ only by the position of one co-ordinated water molecule. The simulated PXRD patterns for the two phases are almost identical, and the experimental PXRD patterns are good matches with the simulated pattern, confirming the high purity of the bulk material (Figure S5). Upon removal of the two co-ordinated water molecules on the $\{Bi_2\}$ node together with the solvent residing within the pores, the two desolvated phases are structurally identical.

The structure of NOTT-220-solv is highly porous, incorporating three distinct interconnected pore channels (denoted as *A*, *B*, *C*) *via* binding of the ligands to the {Bi_2} nodes (Figure 2). Taking account of van der Waals radii, Channel *A*, which is bounded by phenyl rings and carboxylate oxygen atoms, has dimensions of 8.3 x 4.5 Å, while channel *B* is bounded by Bi ions and hydrogen atoms from phenyl ring and has dimensions of 5.3 x 3.5 Å. Channel *C* (1.0 x 3.2 Å) is bounded by Bi ions and phenyl rings. Although Channel *C* is too narrow to allow the guest diffusion, it is inter-connected with Channel *A*, and this allows the diffusion of the guest molecules into Channel *C* via Channel *A*. Channels *A*-*C* account for the 56 % pore voids for this material as calculated by PLATON/SQUEEZE,[14] and are filled by free solvent molecules (DMF and water) which can be removed readily *via* heating in a flow of N_2 gas or under vacuum as confirmed by TGA (Figure S4).

The acetone-exchanged sample, NOTT-220-acetone, was prepared to facilitate complete desolvation by suspending the as-synthesised NOTT-220-solv material in acetone for 10 days with frequent exchange of solvent. The fully desolvated material NOTT-220a was prepared by heating NOTT-220-acetone at 100 ^oC under reduced pressure ($1x10^{-10}$ bar) for 24 h. The permanent porosity of NOTT-220a was confirmed by N_2 sorption isotherms at 77 K, which show reversible type-I adsorption behaviour (Figure 3a). Based upon the N_2 isotherm, the apparent BET surface area of NOTT-220a was estimated to be 1014 m^2g^{-1}. The total micropore volume calculated from maximum N_2 uptake at saturation is 0.39 cm^3g^{-1}, consistent with the total crystallographically-determined pore volume of 0.37 cm^3g^{-1}. The pore volume and BET surface area of NOTT-220a are comparable to some of the light metal based MOFs [*e.g.*, MIL-53(Al),[24] NOTT-300(Al)[25]], and are much higher than the values previously reported for heavy metal based MOFs (*e.g.*, Bi-MOFs[10a-c], U-MOFs[26], Ba-MOFs[27]), but are lower than those of the most porous MOFs based upon Zn(II) or Cu(II) ions.[4] Gravimetric H_2 adsorption isotherms at 77 K show good reversibility and an absence of hysteresis, and give a total storage capacity of 1.5 wt% at 1.0 bar and 2.8 wt% at 20 bar at 77 K (Figure 3b). This uptake is relatively low compared to high performance H_2 storage materials,[6-8] but is consistent with the BET area and pore volume. The heat of adsorption is estimated to be 7.2 kJ mol^{-1} at zero surface coverage (Figure S8), and is within the range (4-8 kJ mol^{-1}) typically observed for MOF materials.[1,2]

CO_2 and CH_4 sorption by NOTT-220a at 195 K shows type-I adsorption characteristics (Figures 3c, 3d). The maximum CO_2 uptake (47 wt% at saturation) was recorded at 195 K and 1.0 bar. At ambient temperatures, the CO_2 storage capacity of NOTT-220a was found to be 40.7 and 37.9 wt% at 273 and 293 K,

respectively. The pore size distribution, estimated from CO_2 adsorption data for NOTT-220a at 273 K, reveals four types of pores with diameters of 4.8, 5.4, 6.1 and 7.8 Å (Figure S6). This is in excellent agreement with the measured channel diameters from the single crystal structures (5-8 Å). The CH_4 uptakes at 20 bar were found to be 14.1 and 8.2 wt% at 195 and 293 K, respectively. The heats of adsorption at zero surface coverage for NOTT-220a are estimated to be 32 and 16 kJ mol^{-1} for CO_2 and CH_4 uptakes, respectively (Figure S8), and are comparable to the values for MOF materials with similar uptakes.[1,2]

Desolvated NOTT-220a has a high bulk density (a crystallographically-determined density) of 1.45 g cm^{-3} (framework-only density 3.17 g cm^{-3}) based upon removal of guest solvents and coordinated water molecules: this value is higher than those of other reported MOFs[4] with comparable or higher porosity and is due to the inclusion of $\{Bi_2\}$ nodes in the framework construction. The volumetric gas uptakes of NOTT-220a were determined based upon the bulk density (1.45 gcm^{-3}) for the desolvated framework. The H_2 uptake of NOTT-220a at 20 bar and 77 K is 42 gL^{-1}, and is comparable to some of the high performance MOFs[4a-c], despite NOTT-220a having a much lower gravimetric uptake. At moderate pressure (20 bar) and ambient temperature (*i.e.* 293 K), the CO_2 uptake of NOTT-220a (553 gL^{-1}) is higher than that of MOF-210 and NU-100 (205 and 332 gL^{-1}, respectively)[4a,4b], but is surpassed by NOTT-122[28a] (also noted as NU-125[28b] and NTU-105[28c]) (616 gL^{-1}), $[Cu_3(BTB)]$ (659 gL^{-1})[29] and USTA-20 (572 gL^{-1})[30] (Table S2). The maximum volumetric CH_4 uptake of NOTT-220a was determined as to be 287 V(STP)/V at 195 K and 20 bar. At 293 K and 20 bar the corresponding CH_4 uptake drops to 165 V(STP)/V, and is higher than the values for all the MOF materials under the same conditions, except for PCN-14[12] which has an uptake of 180 V(STP)/V at 20 bar and 290 K (Table S3).

Significantly, these high uptakes of NOTT-220a are also confirmed by Grand Canonical Monte Carlo (GCMC) simulations which show excellent agreement with the experimental isotherm data, especially for CH_4 (Figure 3d). The discrepancy observed between simulated and experimental isotherms for CO_2 uptake is due to the lack of the accuracy in describing the quadrupole moment of CO_2 molecule, which thus represents a challenge in these simulations. In addition, the preferred positions for adsorbed CH_4 and CO_2 within the framework host were predicted by DFT calculation to be above three oxygen atoms and one bismuth atom at the $\{Bi_2\}$ nodes (Figure S15). The dominating interaction to stabilise CH_4 molecules is weak hydrogen bond between H atoms on CH_4 molecules and oxygen centre from carboxylate group (Figure S15a,b). In contrast, adsorbed CO_2 molecules form dipole interactions between the electropositive carbon

centre and the oxygen centre from the carboxylate group (Figure S15c,d). An estimation of the binding energies of 8.1 kJ/mol for CH_4 and 21 kJ/mol for CO_2 was provided by the DFT calculations. Thus, the observed high uptake capacities and adsorption processes were fully modelled and confirmed from these GCMC and DFT simulations

A CH_4 uptake of 189 V(STP)/V is obtained at 35 bar and 293 K from this modelling study (Figure S12). Interestingly, this material, together with NOTT-122 (NU-125 and NTU-105),[28] Ni-MOF-74,[11] NOTT-107,[9a,31] and PCN-14[12] have the highest volumetric CH_4 uptakes reported to date. Whilst most other MOF systems contain light transition metal ions, such as Cu(II) or Ni(II) as nodes and thus have low framework densities, the incorporation of heavy metal ions (*e.g.* Bi in this study) into the MOF material has advantages in improving their gas storage properties on a volumetric basis. It is worth noting that these volumetric uptake capacities reported here represent the situation of MOFs in their single crystal states and do not take into account any powder packing efficiency in the bulk materials, and therefore the working capacity at practical operation will be reduced accordingly.

Conclusions

In summary, we have synthesised the porous NOTT-220-solv based upon the heavy Bi(III) cations bridged by biphenyl-3,3',5,5'-tetracarboxylate ligands. NOTT-220-solv incorporates a novel binuclear $\{Bi_2\}$ building block and exhibits a new framework topology due to the distorted coordination environment at $\{Bi_2\}$ centres. Although desolvated NOTT-220a exhibits an overall moderate porosity compared to a number of highly porous MOF materials (1014 m^2g^{-1}), it shows good gravimetric gas uptakes, 40.7 and 37.9 wt% at 273 and 293 K for CO_2 and 14.1 and 8.2 wt% at 195 and 293 K for CH_4 at 20 bar. Furthermore, the high crystal density of the desolvated material leads to exceptionally high volumetric uptake capacities, particularly for CH_4 and CO_2, thus representing good potential for volumetric gas storage. Based upon this observation, we will further explore the synthesis of new highly porous MOFs based upon heavy metal ions, coupling high framework density with high porsity thus potentially increased volumetric gas uptake properties.

Acknowledgements

SY gratefully acknowledges receipt of a Leverhulme Trust Early Career Research Fellowship and a Nottingham Research Fellowship, and MS receipt of an ERC Advanced Grant and EPSRC Programme Grant. EB acknowledges EPSRC Career Acceleration Fellowship, New Directions for EPSRC Research Leaders Award (EP/G005060) and ERC Starting Grant for funding. We are grateful of Diamond Light Source for the access to Beamline I19.

List of materials

NOTT-220-solv: $[Bi_2(C_{16}H_6O_6)_{1.5}(H_2O)_2]\cdot(DMF)_{3.5}\cdot(H_2O)_3$ as-synthesised sample.

NOTT-220-acetone: $[Bi_2(C_{16}H_6O_6)_{1.5}(H_2O)_2]\cdot(C_3H_6O)_{2.5}\cdot(H_2O)_{4.5}$ acetone-exchanged sample.

NOTT-220a: $[Bi_2(C_{16}H_6O_6)_{1.5}]$ desolvated sample.

Notes and References

Crystallographic data have been deposited with the Cambridge Crystallographic Data Centre as supplementary publication CCDC 899427 and 899428 for the *alpha* and *beta* phases respectively. ESI is available at XXX containing views of crystal structures, details of gas adsorption data and analyses, TGA, PXRD data and GCMC calculations.

[1] R. J. Kuppler, D. J. Timmons, Q.-R. Fang, J.-R. Li, T. A. Makal, M. D. Young, D. Yuan, D. Zhao, W. Zhuang, H.-C. Zhou, *Coord. Chem. Rev.* **2009**, *253*, 3042–3066.

[2] (a) L. J. Murray, M. Dincă, J. R. Long, *Chem. Soc. Rev.* **2009**, 38, 1294-1314; (b) X. Lin, N. R. Champness and M. Schröder, *Top. Curr. Chem.* **2010,** *293***,** 35-76; (c) K. Konstas, T. Osl, Y. Yang, M. Batten, N. Burke, A. J. Hill, M. R. Hill, *J. Mater. Chem.* **2012**, 22, 16698-16708; (d) T. A. Makal, J.-R. Li, W. Lu, H.-C. Zhou, *Chem. Soc. Rev.* **2012**, *41*, 7761-7779; (e) J.A. Mason, M. Veenstra, J.R. Long, *Chem. Sci.* **2014**, **5**, 32-51.

[3] (a) K. Sumida, D. L. Rogow, J. A. Mason, T. M. McDonald, E. D. Bloch, Z. R. Herm, T.-H. Bae, J. R. Long, *Chem. Rev.* **2012**, *112*, 724–781. (b) J. M. Simmons, H. Wu, W. Zhou, T. Yildirim, *Energy Environ. Sci.* **2011**, *4*, 2177-2185.

[4] (a) O. K. Farha, A. Özgür Yazaydın, I. Eryazici, C. D. Malliakas, B. G. Hauser, M. G. Kanatzidis, S. T. Nguyen, R. Q. Snurr, J. T. Hupp, *Nature Chem.* 2010, ***2***, 944–948; (b) H. Furukawa, N. Ko, Y. B. Go, N. Aratani, S. B. Choi, E. Choi, A. O. Yazaydin, R. Q. Snurr, M. O'Keeffe, J. Kim, O. M. Yaghi, *Science* **2010**, *329*, 424–428; (c) Y. Yan, S. Yang, A. J. Blake, W. Lewis, E. Poirier, S. A. Barnett, N. R. Champness, M. Schröder, *Chem. Commun.* **2011**, *47*, 9995-9997; (d) Y. Yan, I. Telepeni, S. Yang, X. Lin, W. Kockelmann, A. Dailly, A.J. Blake, W. Lewis, G. S Walker, D. R. Allan, S. A. Barnett, N. R. Champness, M. Schröder, *J. Am. Chem. Soc.* **2010**, *132*, 4092–4094; (e) H. Deng, S. Grunder, K. E.

Cordova, C. Valente, H. Furukawa, M. Hmadeh, F. Gandara, A. C. Whalley, Z. Liu, S. Asahina, H. Kazumori, M. O'Keeffe, O. Terasaki, J. F. Stoddart, O. M. Yaghi, *Science* **2012**, *336*, 1018–1023.

[5] (a) S. T. Zheng, Y. Li, T. Wu, R. A. Nieto, P. Feng, X. Bu, *Chem. Eur. J.* **2010**, *16*, 13035–13040; (b) X. Liu, G. C. Guo, B. Liu, W. T. Chen, J. S. Huang, *Cryst. Growth & Des.* **2005**, *5*, 841–843; (c) X. Liu, G.-C. Guo, A.-Q. Wu, J.-S. Huang, *Inorg. Chem. Commun.* **2004**, *7*, 1261–1263.

[6] (a) K. Sumida, M. R. Hill, S. Horike, A. Dailly, J. R. Long, *J. Am. Chem. Soc.* **2009**, 131, 15120–15121; (b) X. Luo, D. Luo, H. Zeng, M. Gong, Y. Chen, Z. Lin, *Inorg. Chem.* **2011**, *50*, 8697–8699; (c) M. Kang, D. Luo, X. Luo, Z. Chen, Z. Lin, *CrystEngComm*. **2011**, *14*, 95-97.

[7] (a) D. Britt, H. Furukawa, B. Wang, T. G. Glover, O. M. Yaghi, *Proc. Natl. Acad. Sci. U.S.A*. **2009**, *106*, 20637–20640; (b) M. Dincă, J. R. Long, *J. Am. Chem. Soc*. **2005**, *127*, 9376–9377

[8] M. P. Suh, H. J. Park, T. K. Prasad, D.-W. Lim, *Chem. Rev*. **2012**, *112*, 782–835.

[9] (a) X. Lin, I. Telepeni, A.J. Blake, A. Dailly, C.M. Brown, J. M. Simmons, M. Zoppi, G. S. Walker, K.M. Thomas, T.J. Mays, P. Hubberstey, N.R. Champness, M. Schröder, *J. Am. Chem. Soc*. **2009**, *131*, 2159-2171; (b) W. Yang, A. Greenaway, X. Lin, R. Matsuda, A. J. Blake, C. Wilson, W. Lewis, P. Hubberstey, S. Kitagawa, N. R. Champness, M. Schröder, *J. Am. Chem. Soc.* **2010**, *132*, 14457–14469; (c) S. Yang, S. K. Callear, A. J. Ramirez-Cuesta, W. I. F. David, J. Sun, A. J. Blake, N. R. Champness, M. Schröder, *Faraday Discuss.* **2011**, *151*, 19-36.

[10] (a) A. Thirumurugan, W. Li, A. K. Cheetham, *Dalton Trans.* **2012**, *41*, 4126–4134; (b) A. Thirumurugan, A. K. Cheetham, *Eur. J. Inorg. Chem.* **2010**, 3823–3828; (c) A. C. Wibowo, S. A. Vaughn, M. D. Smith, H.-C. zur Loye, *Inorg. Chem.* **2010**, *49*, 11001–11008; (d) M. Feyand, E. Mugnaioli, F. Vermoortele, B. Bueken, J. M. Dieterich, T. Reimer, U. Kolb, D. de Vos, N. Stock, *Angew. Chem. Int. Ed.* **2012**, *51*, 10373–10376; (e) M. Feyand, M. Köppen, G. Friedrichs, N. Stock, *Chem.-Eur. J.* **2013**, *19*, 12537–12546; (f) V. Chandrasekhar, R. K. Metre, *Dalton Trans.* **2012**, *41*, 11684; (g) A. C. Wibowo, M. D. Smith, J. Yeon, P. S. Halasyamani, H.-C. zur Loye, *J. Solid State Chem.* **2012**, *195*, 94–100.

[11] H. Wu, W. Zhou, T. Yildirim, *J. Am. Chem. Soc.* **2009**, *131*, 4995–5000.

[12] S. Ma, D. Sun, J. M. Simmons, C. D. Collier, D. Yuan, H.-C. Zhou, *J. Am. Chem. Soc*. **2008**, *130*, 1012–1016.

[13] G. M. Sheldrick, *Acta Crystallogr. Sect. A* **2008**, *64*, 112.

[14] A. L. Spek, *Acta Crystallogr. Sect. D* **2009**, *65*, 148.

[15] A. Gupta, S. Chempath, M. J. Sanborn, L. A. Clark, R. Q. Snurr, *Mol. Simul*. **2003**, *29*, 29-46.

[16] M. J. Martin, J. I. Siepmann, *J. Phys. Chem. B* **1998**, *102*, 2569-2577.

[17] W. L. Jorgensen, D. S. Maxwell, J. Tirado-Riveset, *J. Am. Chem. Soc.* **1996,** *118,* 11225-11236.

[18] A. K. Rappe, C. J. Casewit, K. S. Colwell, W. A. Goddard III, W. M. Skid, *J. Am. Chem. Soc*. **1992**, *114*, 10024-10035.

[19] Q. Yang, C. Zhong, *J. Phys. Chem. B* **2006***, 110,* 655-658.

[20] D-Y. Peng, D. B. Robinson, *Ind. Eng. Chem. Fund.* **1976**, 15, 59-64.

[21] Y. Shao *et al*. *Phys. Chem. Chem. Phys*. **2006**, *8*, 3172-3191.

[22] C. M. Breneman and K. B. Wiberg, *J. Comput. Chem.* **1990**, *11*, 361-373.

[23] V. A. Blatov, *IUCr CompComm Newsletter* **2006**, *7*, 38-143.

[24] T. Loiseau, C. Serre, C. Huguenard, G. Fink, F. Taulelle, M. Henry, T. Bataille, G. Férey, *Chem. Eur. J.* **2004**, *10*, 1373–1382.

[25] S. Yang, J. Sun, A.J. Ramirez-Cuesta, S.K. Callear, W.I.F. David, D.P. Anderson, R. Newby, A.J. Blake, J.E. Parker, C.C. Tang, M. Schröder, *Nature Chem.* **2012**, 4, 887-894.

[26] (a) J. Y. Kim, A. J. Norquist, D. O'Hare, *Dalton Trans.* **2003**, 2813–2814 ; (b) C. Volkringer, I. Mihalcea, J.-F. Vigier, A. Beaurain, M. Visseaux, T. Loiseau, *Inorg. Chem.* **2011**, *50*, 11865–11867.

[27] M. L. Foo, S. Horike, Y. Inubushi, S. Kitagawa, *Angew Chem. Int. Ed.* **2012**, *51*, 6107–6111.

[28] (a) Y. Yan, M. Suyetin, E. Bichoutskaia, A. J. Blake, D. R. Allan, S. A. Barnett, M. Schröder, *Chem. Sci.* **2013**, *4*, 1731-1736; (b) C. E. Wilmer, O. K. Farha, T. Yildirim, I. Eryazici, V. Krungleviciute, A. A. Sarjeant, R. Q. Snurr, J. T. Hupp, *Energy Environ. Sci.* **2013**, *6*, 1158-1163; (c) X.-J. Wang, P.-Z. Li, Y. Chen, Q. Zhang, H. Zhang, X. X. Chan, R. Ganguly, Y. Li, J. Jiang, Y. Zhao, *Sci. Rep.* **2013**, *3*, 12012

[29] B. Zheng, Z. Yang, J. Bai, Y. Li, S. Li, *Chem. Commun.* **2012**, *48*, 7025-7027.

[30] Z. Guo, H. Wu, G. Srinivas, Y. Zhou, S. Xiang, Z. Chen, Y. Yang, W. Zhou, M. O'Keeffe, B. Chen, *Angew. Chem. Int. Ed.* **2011**, *50*, 3178–3181.

[31] C. E. Wilmer, M. Leaf, C. Y. Lee, O. K. Farha, B. G. Hauser, J. T. Hupp, R. Q. Snurr, *Nature Chem.* **2012**, 4, 83–89.

Figures and Schemes:

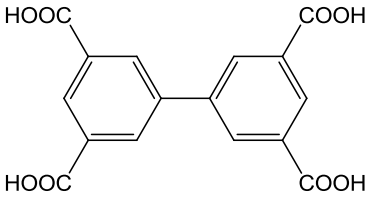

Scheme 1. View of biphenyl-3,3',5,5'-tetracarboxylic acid (H_4L)

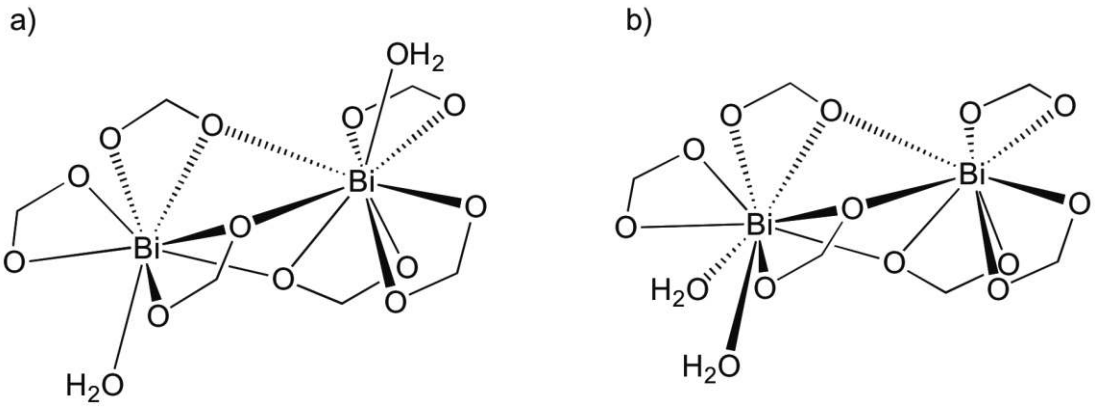

Scheme 2. a) Coordination geometry of *alpha*-NOTT-220-solv showing a water molecule bound to each Bi(III) centre; b) coordination geometry of *beta*-NOTT-220-solv showing two water molecules coordinated to the same Bi(III) centre.

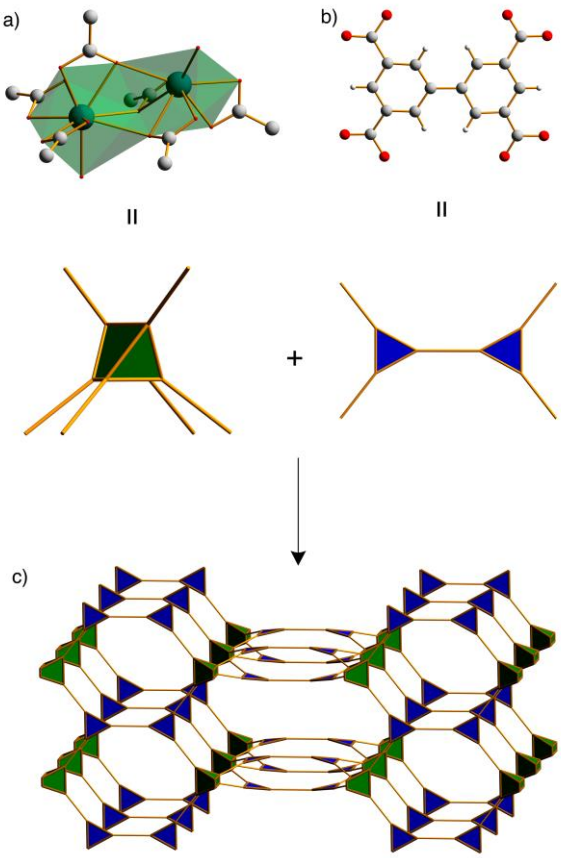

Figure 1. a) b) View of building blocks within NOTT-220-solv (C, white; O, red; Bi, green). c) Assembly of building blocks into the idealised augmented net of $\{4\cdot6^2\}_2\{4^2\cdot6^5\cdot8^8\}\{6^2\cdot8\}$ point symbol.

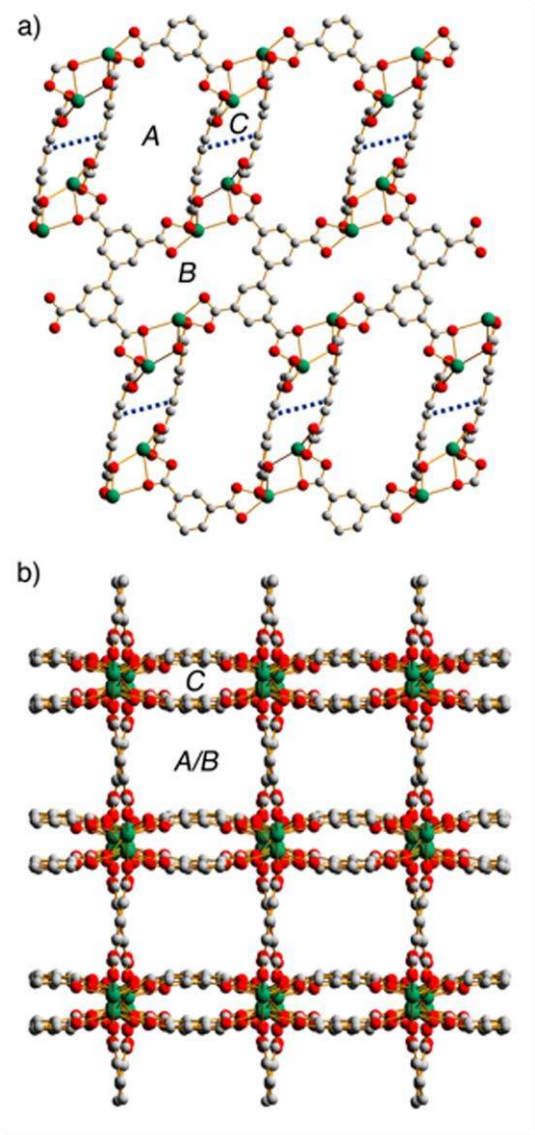

Figure 2. a) View of the crystal structure of NOTT-220-solv along the crystallographic *c* axis. The offset face to face π-π stacking (highlighted in blue) of the L^{4-} ligand is shown in channel *C*. b) View along the crystallographic [201] direction showing rectangular pore channels as a result of the π-π interaction between the ligand molecules.

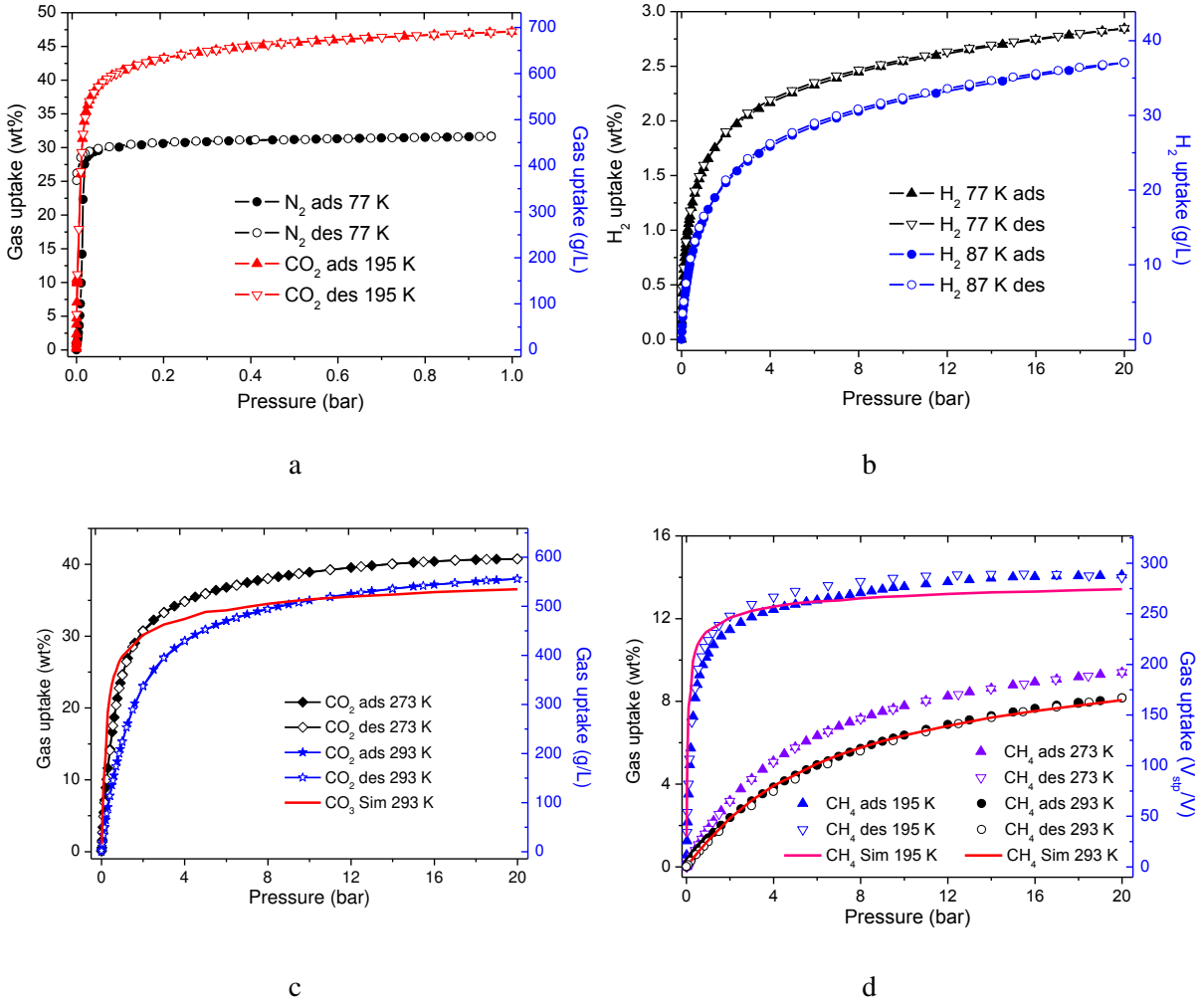

Figure 3. Gas adsorption isotherms for desolvated NOTT-220a. (a) N_2 isotherms at 77 K and CO_2 isotherms at 195 K up to 1.0 bar; (b) H_2 isotherms at 77 and 87 K up to 20 bar; (c) CO_2 experimental and simulated isotherms at 273 and 293 K up to 20 bar; (d) CH_4 experimental and simulated isotherms at 195, 273, and 293 K up to 20 bar.

Table of Contents Graphic

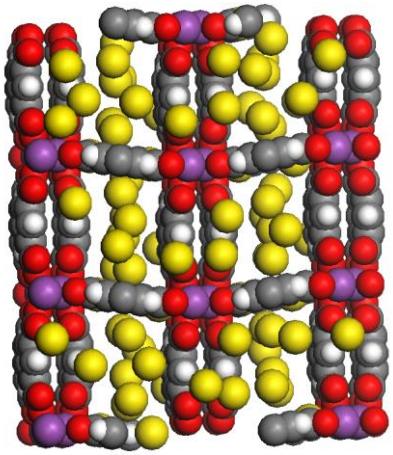

The 3,6-connected material $[Bi_2(L)_{1.5}(H_2O)_2]\cdot(DMF)_{3.5}\cdot(H_2O)_3$ (NOTT-220-solv) (L = biphenyl-3,3',5,5'-tetracarboxylate) shows a new framework topology with a $\{4\cdot6^2\}_2\{4^2\cdot6^5\cdot8^8\}\{6^2\cdot8\}$ point symbol. The desolvated material NOTT-220a shows a maximum CH_4 uptake of 287 V(STP)/V at 20 bar, 195 K with a CO_2 uptake of to 688 gL^{-1} at 1 bar, 195 K.

Electronic Supplementary Information

A Novel Bismuth-Based Metal-Organic Framework for High Volumetric Methane and Carbon Dioxide Adsorption

Mathew Savage,[1] Sihai Yang,[1] Mikhail Suyetin,[1] Elena Bichoutskaia,[1] Alexander J. Blake,[1] Sarah A. Barnett[2] and Martin Schröder[1]*

1. Mr. M. Savage, Dr. S. Yang, Dr. M. Suyetin, Dr. E. Bichoutskaia, Prof. Dr. A.J. Blake, Prof. Dr. M. Schröder, School of Chemistry, University of Nottingham, University Park, Nottingham NG7 2RD (UK) Fax: +44 115 9513563; Tel: +44 115 9513490; E-mail: M.Schroder@nottingham.ac.uk.
2. Dr. S.A. Barnett, Diamond Light Source, Harwell Science and Innovation Campus, Didcot, Oxfordshire, OX11 0DE (UK)

Additional Experimental Details

Materials and Measurements

Bismuth nitrate pentahydrate 99.999 %, piperazine 99 %, 3,3',5,5'-tetramethyl biphenyl 97+ %, and potassium permanganate 98 % were purchased from Alfa Aesar (VWR). Dimethyl formamide, acetonitrile, *tert*-butanol, sodium hydroxide and *conc.* nitric and hydrochloric acid were purchased from Fischer scientific. All reagents and solvents were used without further purification. Elemental analyses (C, H, and N) were carried out on a CE-440 elemental analyzer. Thermal gravimetric analyses (TGA) were performed under nitrogen flow (100 ml/min) with a heating rate of 5 °C/min using a Perkin Elmer Pyris 1 thermogravimetric analyser. Fourier transform infrared spectroscopy (FTIR) spectra were recorded using a Nicolet Avatar 360 FT-IR spectrophotometer in the 4000~400 cm^{-1} range. Powder X-ray diffraction (PXRD) data were collected over the 2θ range 2-40^o on a PANalytical X'pert diffractometer using Cu-$K_{\alpha 1}$ radiation (λ = 1.5406 Å) at 40 kV and 40mA. PXRD data were collected using flat plate mode, and preferred orientation effects are responsible for the strong intensity observed for specific reflections. Grinding samples however leads to serious solvent loss and partial decomposition of the framework in air.

Synthesis of biphenyl-3,3',5,5'-tetracarboxylic acid (H_4L)

H_4L was prepared according to a procedure previously reported by our group.[1] 3,3',5,5'-tetramethyl biphenyl (15 g, 0.069 mol) and NaOH (6.0 g, 0.15 mol) were dissolved in a mixture of *tert*-butanol and water (1:1 *v/v* 500 mL) and heated to 50 °C. Potassium permanganate (129 g, 0.81 mmol) was added in portions over a period of a week, when the reaction mixture was purple for more than 1 day, the reaction mixture was filtered until clear, cooled in an ice bath and acidified with *conc.* hydrochloric acid (37 %, 50 mL). The white precipitate was collected by filtration and recrystallized from DMF to yield biphenyl-3,3',5,5'-tetracarboxylic acid (H_4L), as a pure white powder (16.2 g, 0.049 mol, 71 % yield). Elemental analysis (% calc/found): $C_{16}H_{10}O_8$ (C 58.19/56.95, H 3.05/3.24, N 0/0.69). Crystallisation solvents of 0.17 DMF and 0.31 H_2O can account for the discrepancy in elemental analysis data. ^{1}H NMR (MeOD, 300 MHz): 8.64 (1H, t, *J*) 1.8 Hz); 8.49 (2H, s); 4.39 (4H, q, *J* 6.9Hz),1.43(6H, t, *J* 7.2Hz).

Additional views of the X-ray crystal structure of NOTT-220-solv.

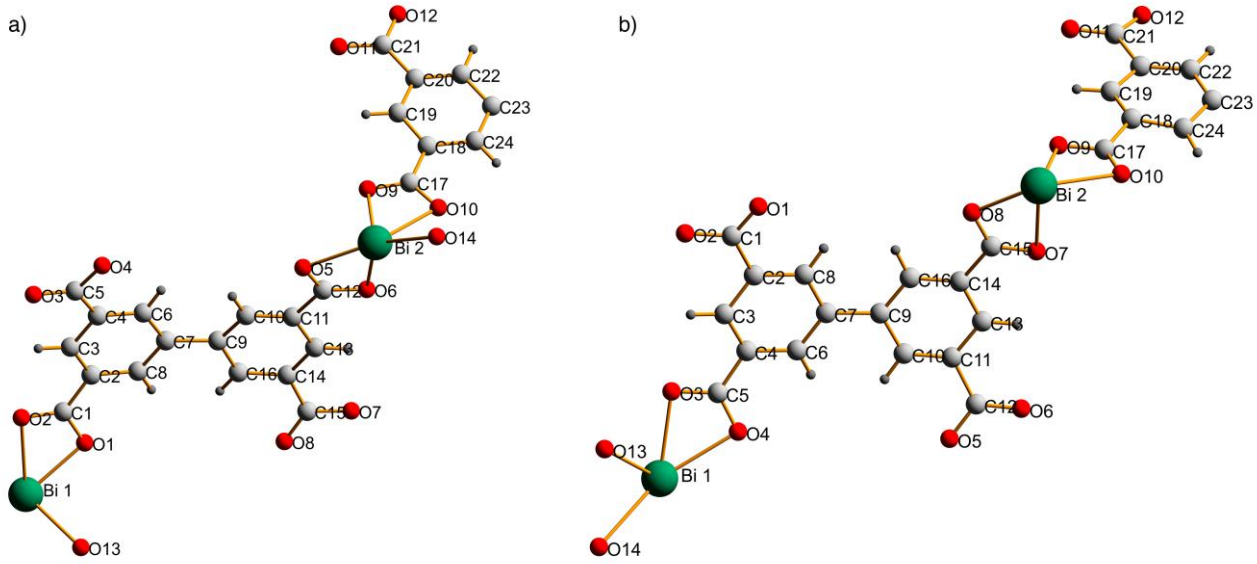

Figure S1**.** Views of the asymmetric units of the a) *alpha* and b) *beta* phase of NOTT-220-solv. (Bi, green; carbon, white; oxygen, red; hydrogen, grey).

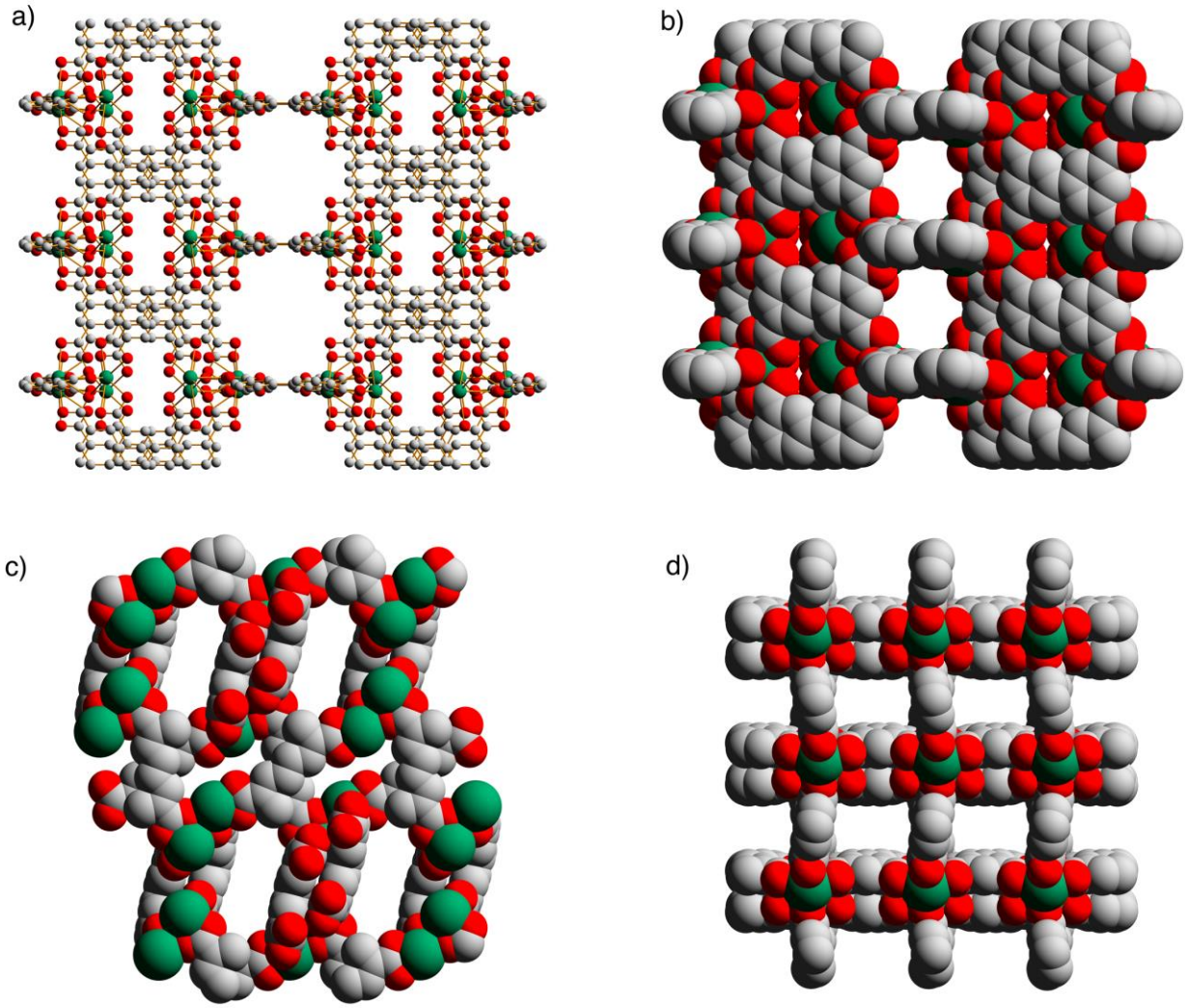

Figure S2. a) Ball and stick representation of NOTT-220-solv viewed along the crystallographic *c* axis; b), c) and d) space-filling representations of NOTT-220-solv viewed along the crystallographic *c*, *b* and [201] directions, respectively. (Bi, green; carbon, white; oxygen, red; hydrogen atoms are omitted for clarity).

Topology and simplification of NOTT-220

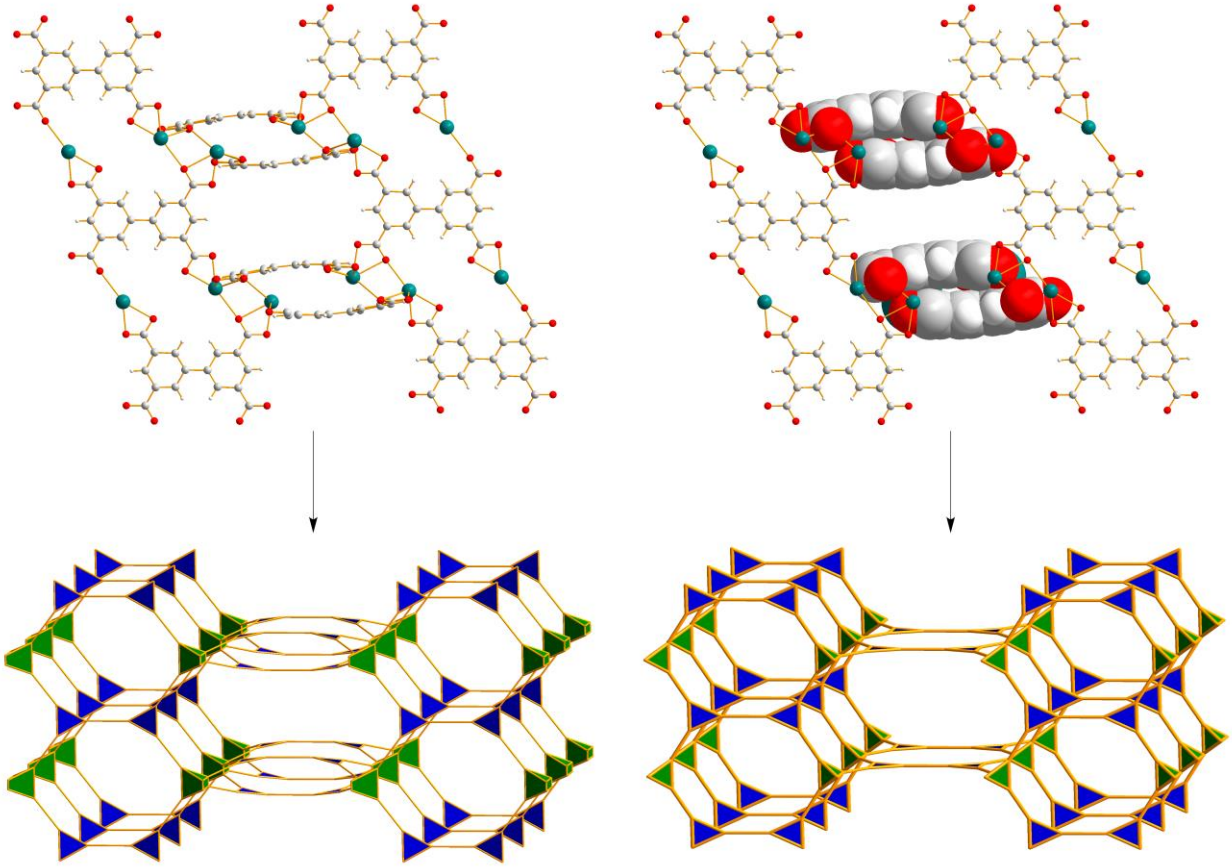

$\{4\cdot6^2\}_2\{4^2\cdot6^5\cdot8^8\}\{6^2\cdot8\}$ $\{6^2,8^4\}\{6^2,8\}$ – **tfi**

a) b)

Figure S3. Comparison of crystal structure of NOTT-220 with the augmented net. a) Ball and stick representation of NOTT-220 indicating the direct mapping of ligands and metal nodes to the augmented net of $\{4\cdot6^2\}_2\{4^2\cdot6^5\cdot8^8\}\{6^2\cdot8\}$ topology. b) Ball and stick representation of NOTT-220 featuring a spacefilling diagram for the central π-stacked ligands. If this pair is considered as a single vertex, the structure can map onto the augmented net of the $\{6^2,8^4\}\{6^2,8\}$ (**tfi**) topology.

TGA plot for NOTT-220-solv.

The uncoordinated solvent molecules in NOTT-220-solv can be readily exchanged for acetone, and removed by heating at 100°C either under a flow of N_2 gas or *in vacuo*. TGA measurements show that the as-synthesised sample loses solvent slowly between 20 and 270 °C, while the acetone-exchanged sample loses solvent rapidly between 20 and 80 °C, giving fully desolvated material NOTT-220a. This is followed by a significant loss at *ca.* 360 °C, corresponding to the decomposition of the framework (Figure S3). The weight loss of 28.0 wt% from the as synthesized NOTT-220-solv between 20 and 270 °C correlates with solvent loss based upon 3.5 DMF and 5 water molecules per bismuth node (cal. 28.7 wt%). The weight loss of 18 % from the acetone exchanged sample of NOTT-220-acetone correlates with a loss of solvent based upon 2.5 acetone and 4.5 water molecules per bismuth node (cal. 20.8 wt%). The volatility of crystallization solvents in the samples contributes to the discrepancies between room temperature and 300°C.

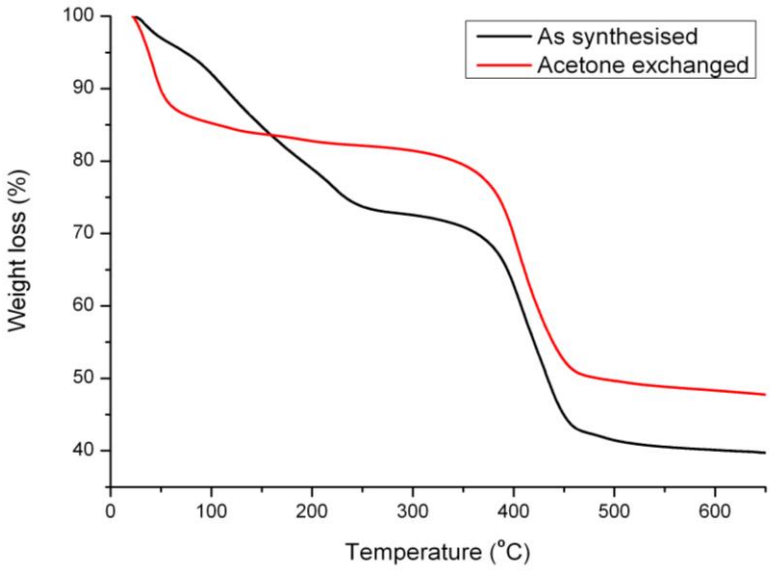

Figure S4. Comparison of TGA plots for as synthesized sample of NOTT-220-solv and acetone exchanged sample of NOTT-220-acetone.

Powder X-ray diffraction for NOTT-220-solv.

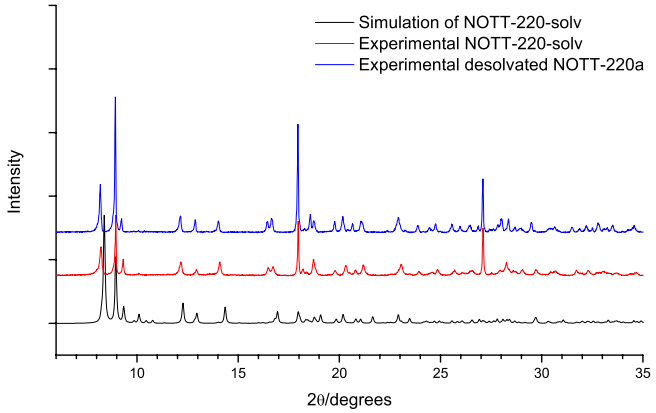

Figure S5. Comparison of simulated and experimental PXRD patterns of the as-synthesised and activated material.

Pore Size Distribution Data.

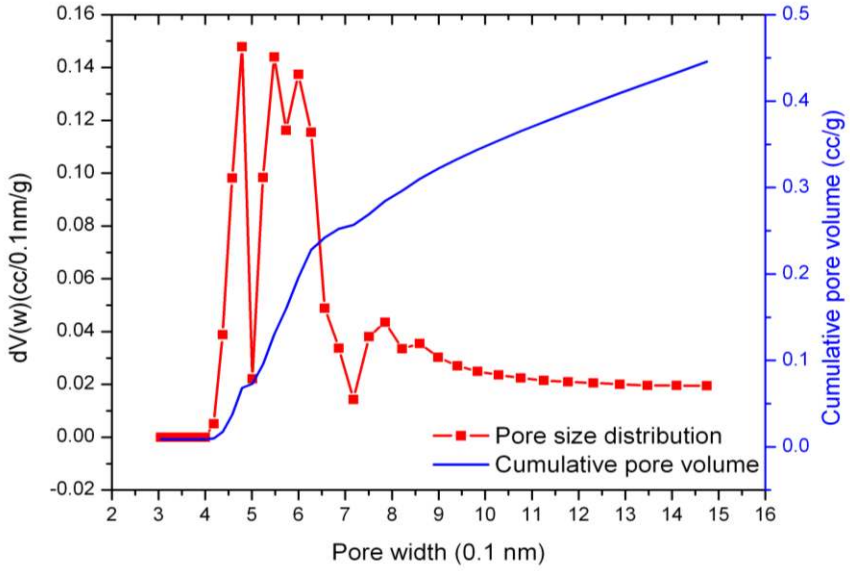

Figure S6. Pore size distribution (left axis, red curve) and cumulative pore volume (right axis, blue curve) for NOTT-220a calculated from a DFT/Monte Carlo fitting of the CO_2 adsorption data at 273 K.

Analysis of isosteric adsorption enthalpy.

The isosteric heat of adsorption Q_{st} was determined by the virial equation (1) from H_2 adsorption isotherms at 77 and 87 K; CO_2 adsorption isotherms at 273 K and 293 K; CH_4 adsorption isotherms at 273 K and 293 K (Figure S6).[2,3]

$$\ln(p) = \ln(n) + \frac{1}{T}\sum_{i=0}^{m} a_i n^i + \sum_{j=0}^{n} b_j n^j \qquad (1)$$

where p is the pressure expressed in mbar, n is the amount adsorbed in mmol/g, T is the temperature in K, a_i and b_j are virial coefficients, and m, n represent the number of coefficients. The values of the virial coefficients a0 through am were then used to calculate the isosteric heat of adsorption using equation (2). Q_{st} is the coverage-dependent isosteric heat of adsorption and R is the universal gas constant.

$$Q_{st} = -R\sum_{i=0}^{m} a_i n^i \quad (2)$$

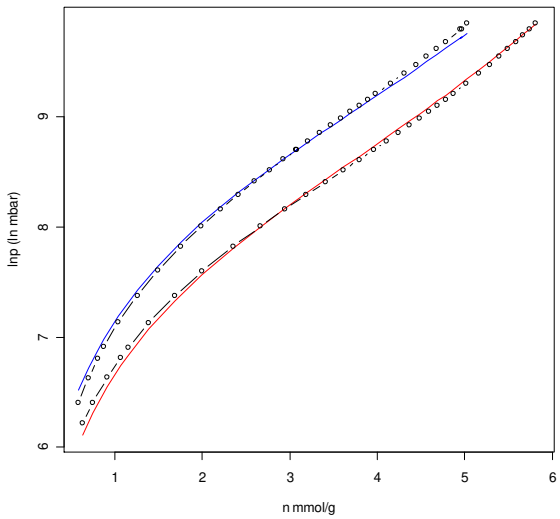

a

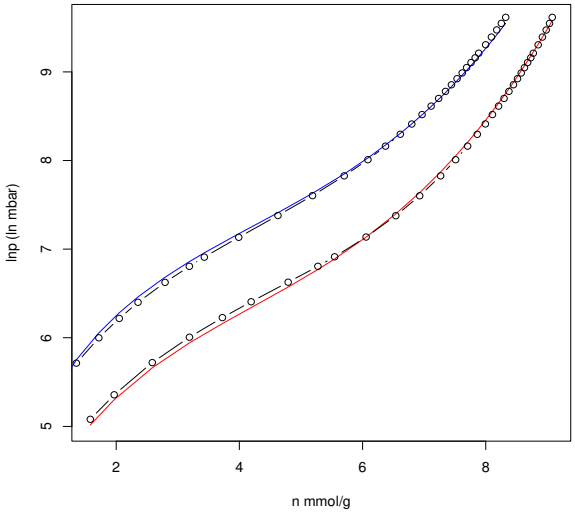

b

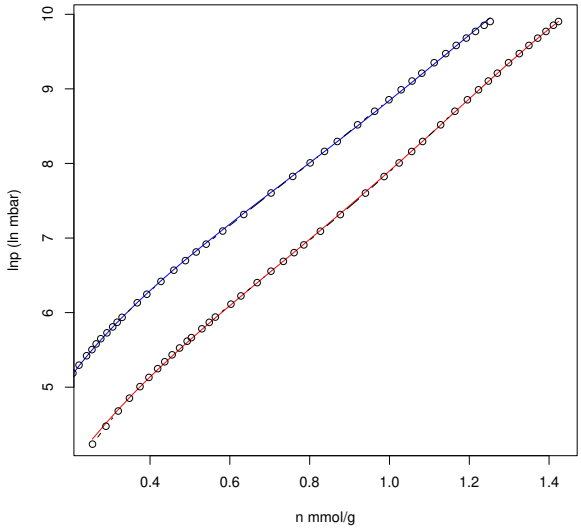

c

Figure S7. Virial expression fitting graphs of CH_4 (a) and CO_2 (b) at 273 K (red) and 293 K (blue), and H_2 (c) at 77 K (red) and 88 K (blue) (a): fitting error=0.048, R^2=0.999, (b): fitting error = 0.040, R^2=0.999, (c) fitting error=0.018, R^2=0.999.

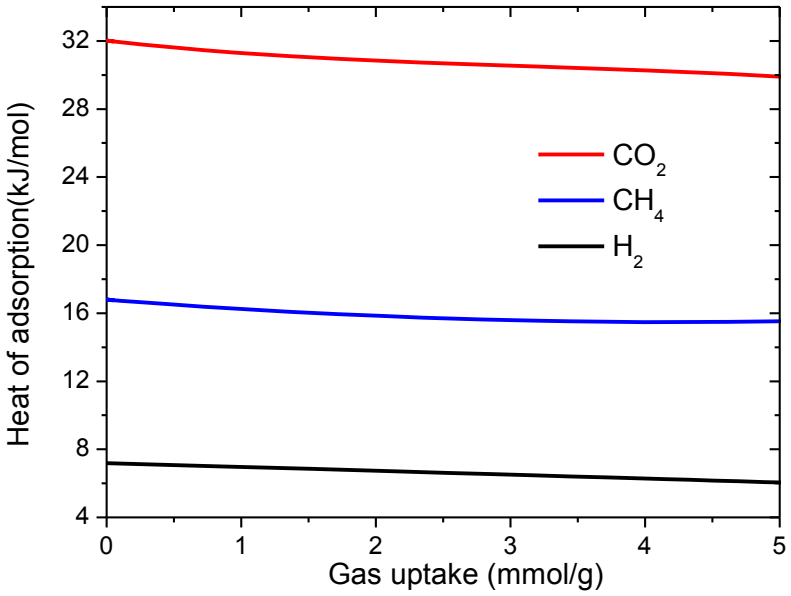

Figure S8 isosteric heat of adsorption of CO_2, CH_4 and H_2

Analysis of gas adsorption selectivity data.

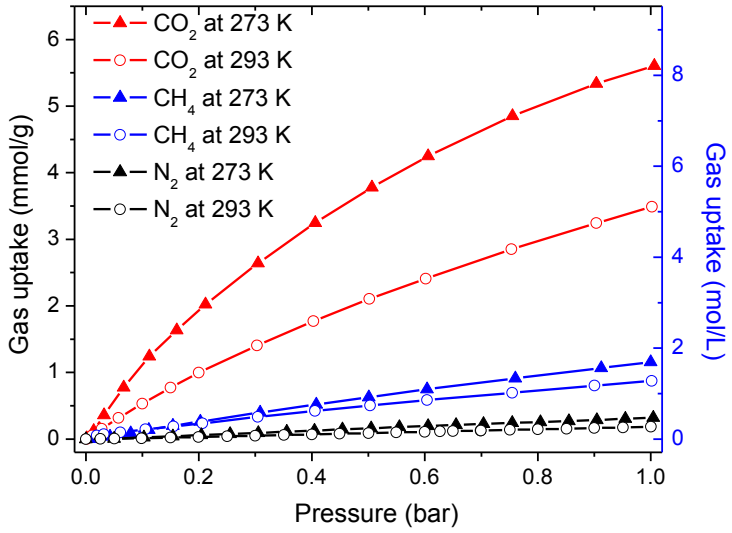

Figure S9. Comparison of the ambient pressure CO_2, CH_4, and N_2 isotherms at 273 and 293 K.

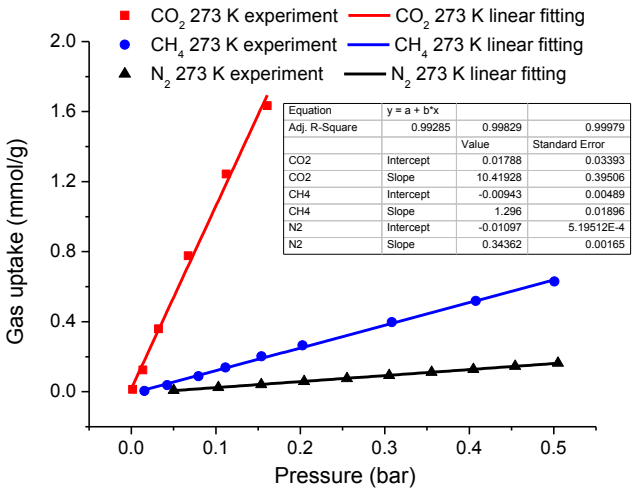

Equation	y = a + b*x		
Adj. R-Square	0.99285	0.99829	0.99979
		Value	Standard Error
CO2	Intercept	0.01788	0.03393
CO2	Slope	10.41928	0.39506
CH4	Intercept	-0.00943	0.00489
CH4	Slope	1.296	0.01896
N2	Intercept	-0.01097	5.19512E-4
N2	Slope	0.34362	0.00165

Figure S10. Linear fitting of CO_2, CH_4 and N_2 isotherms at 273K.

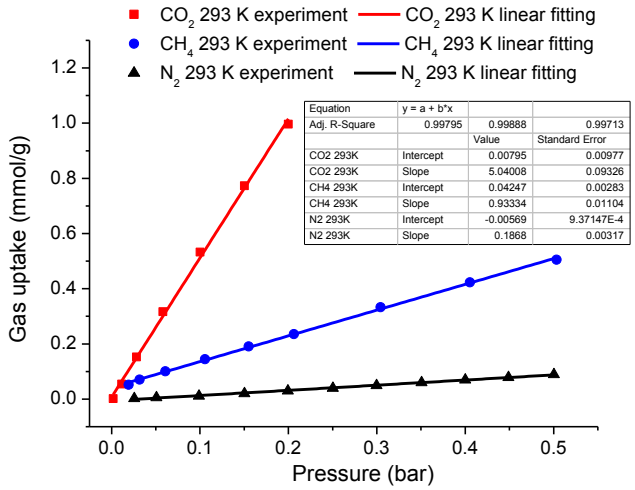

Figure S11. Linear fitting of CO_2, CH_4 and N_2 isotherms at 293K.

Table S1. Selectivity data for NOTT-220 at 273 and 293 K.

	273 K	293 K
CO_2/N_2	31	27
CO_2/CH_4	8.0	5.4
CH_4/N_2	3.8	5.0

Data obtained by comparison of the slopes for initial isotherm plots.

In addition to the excellent volumetric gas uptakes at high pressure, NOTT-220a also exhibits selective CO_2 uptakes at ambient pressure and temperatures. Comparison of the isotherm plots for CO_2, CH_4, and N_2 uptakes up to 1.0 bar yields CO_2/N_2 selectivity ratios of 31, and CO_2/CH_4 selectivity ratios of 8.0 at 273 K (Table S1). These selectivity data are higher than those observed in large-pore materials such as NOTT-202,[5] (CO_2/CH_4: 2.9; CO_2/N_2: 27 at 273 K) but are lower than those of the best-behaving materials (*e.g.*, NOTT-300 CO_2/CH_4: 100; CO_2/N_2: 180 at 273 K).[6]

Grand Canonical Monte Carlo (GCMC) simulations

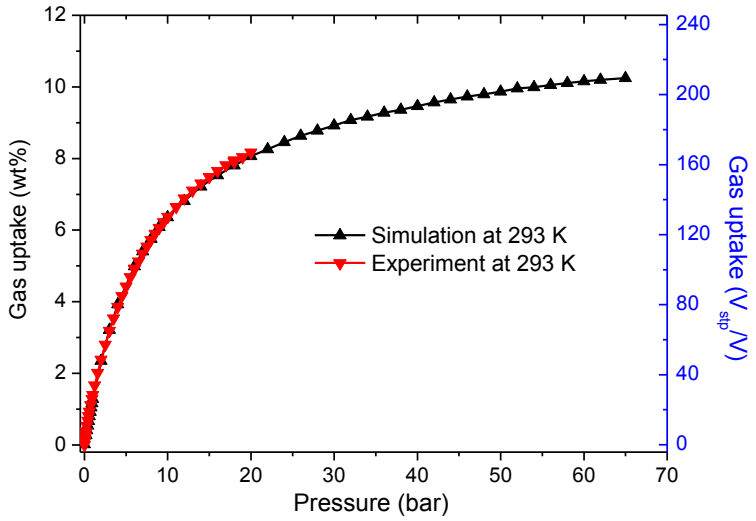

Figure S12. Comparison of the simulated and experimental adsorption isotherms for CH_4 in NOTT-220a at 293 K. Good agreements between the experiment and simulation are observed up to 20 bar, confirming the reliability of the simulation.

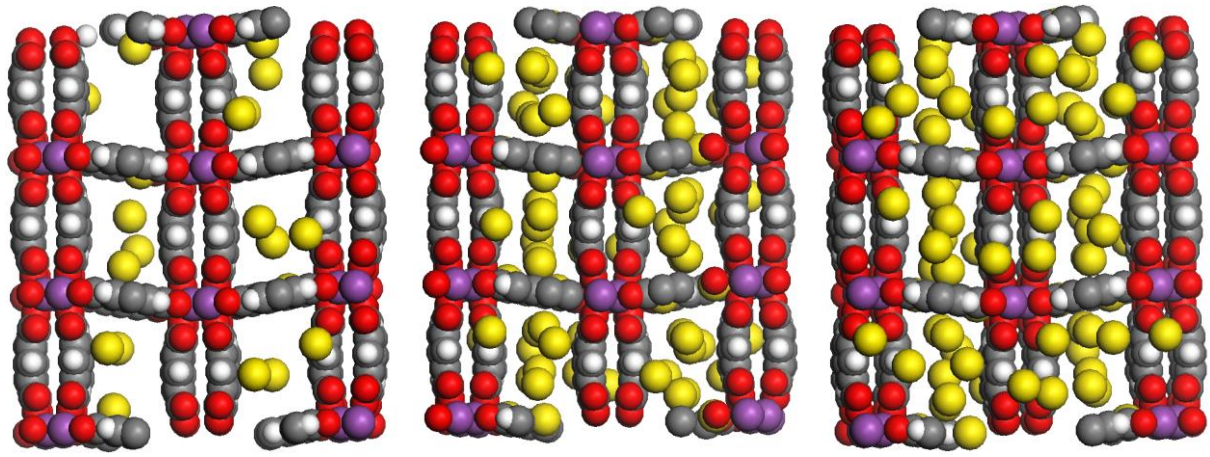

a b c

Figure S13. GCMC modelling of adsorption of CH_4 molecules (yellow spheres) into NOTT-220a at 195 K and 1bar (a), 10 bar (b) and 20 bar (c). (Bismuth: purple; oxygen: red; carbon: grey; hydrogen: white)

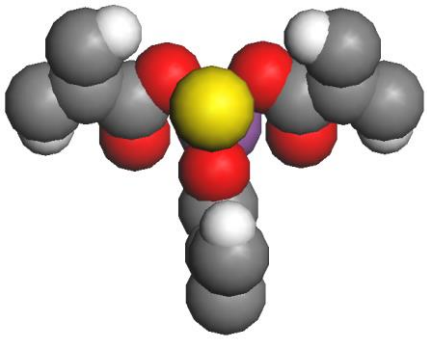

Figure S14. View of the location of CH_4 molecule (yellow sphere), determined by GCMC modelling, above three oxygen atoms and bismuth atom in NOTT-220a, representing the most preferable position for CH_4. (Bismuth: purple; oxygen: red; carbon: grey; hydrogen: white)

Binding energy calculations

Calculations of binding energy between CH_4 and CO_2 with the node of the NOTT-220a have been performed in two-stages: the geometry optimization was done at the B3LYP/6-31G** level of theory, and the binding energies were subsequently calculated at the higher B3LYP /6-311++G** level as follows BE = E(complex) - E(linker) - $E_{opt}(CH_4)$. Both stages were performed with taking into account the dispersion correction proposed by Grimme.[3] The BEs have been corrected for basis set superposition error (BSSE). All DFT calculations were performed with Q-Chem quantum chemistry package.[4]

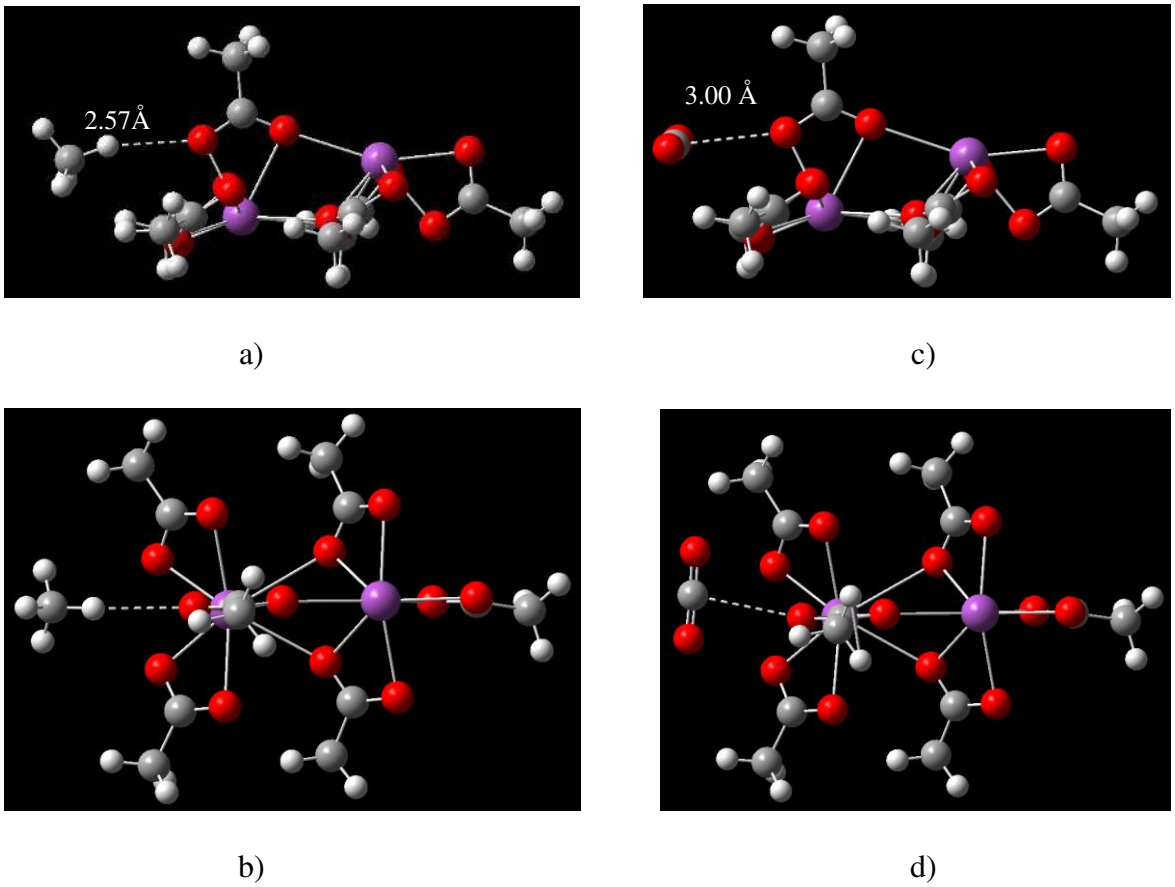

Figure S15. View of the preferred binding mode of CH_4 (a) and b); and CO_2 (c) and d) on the binuclear $\{Bi_2\}$ node of NOTT-220a. a) and c) show the side-on view while b) and d) show the top-down view.

Comparison of the volumetric carbon dioxide uptakes in different MOF systems

Table S2. Summary of volumetric uptakes of CO_2 in different MOF systems at ambient temperatures.

Material	Density	Temperature	CO_2 Uptake		Reference
			20 Bar	High pressure	
	g/cm^3	K	gL^{-1}	gL^{-1}	
NOTT-122/NU-125/NTU-105	0.56	298	684	700[a]	2, 7
$[Cu_3(BTB)]$	0.42	273	659		8
USTA-20	0.90	300	572	590[b]	9
NOTT-220	1.45	293	553		This Work
HKUST-1	0.88	303	502	545[c]	10
MOF-177	0.42	298	487	593[d]	11
MOF-205	0.37	298	473	643[c]	11
NU-100	0.29	298	332	707[e]	12
MOF-210	0.24	298	205	737[c]	11

[*a*] 25 Bar, [*b*] 35 Bar, [*c*] 57 Bar, [*d*] 45 Bar, [*e*] 40 Bar

- * Data reported in this table represent the situation of MOFs in their single crystal state and do not take into account of the powder packing efficiency of the bulk materials

Comparison of the volumetric methane uptakes in different MOF systems

Table S3. Summary of volumetric uptakes of CH_4 in different MOF systems at ambient temperatures.

Material	Density	Temperature	CH_4 Uptake		Reference
			20 Bar	35 Bar	
	g/cm^3	K	V(STP)/V	V(STP)/V	
PCN-14	0.87	290	180	230	13
Ni-MOF-74	1.20	298	165	190	14
NOTT-220	1.46	293	165	189	This work
NOTT-107	0.81	298	143	185	1,15
NOTT-122/NU-125/NTU-105	0.56	298	135	180	2, 7
USTA-20	0.90	298	157	178	7
Co-MOF-74	1.16	298	160	174	14
HKUST-1	0.52	304	152	165	10
ZnTBCPPM	0.68	298	119	160	16
MIL-53 (Al)	0.42	298	132	155	17
PCN-61	0.56	298	112	145	18
MOF-5	0.59	298	75	110	19
PCN-68	0.38	298	66	99	9

- Data reported in this table represent the situation of MOFs in their single crystal state and do not take into account of the powder packing efficiency of the bulk materials.

References

1. X. Lin, I. Telepeni, A. J. Blake, A. Dailly, C. M. Brown, J. M. Simmons, M. Zoppi, G. S. Walker, K. M. Thomas, T. J. Mays, P. Hubberstey, N.R. Champness and M. Schröder, *J. Am. Chem. Soc* **2009**, *131*, 2159–2171.
2. Y. Yan, M. Suyetin, E. Bichoutskaia, A. J. Blake, D. R. Allan, S. A. Barnett, M. Schröder, *Chem. Sci.* **2013**, *4*, 1731-1736.
3. S. Grimme, J. Antony, S. Ehrlich, H. Krieg, *J. Chem. Phys*. **2010**, *132*, 154104.
4. Y. Shao *et al*., *Phys. Chem. Chem. Phys*. **2006**, *8*, 3172-3191.
5. S. Yang, X. Lin, W. Lewis, M. Suyetin, E. Bichoutskaia, J. E. Parker, C. C. Tang, D. R. Allan, P. J. Rizkallah, P. Hubberstey, N.R. Champness, K.M. Thomas, A.J. Blake and M. Schröder, *Nat Mater* **2012**, *11*, 710–716.
6. S. Yang, J. Sun, A. J. Ramirez-Cuesta, S. K. Callear, W. I. F. David, D. P. Anderson, R. Newby, A. J. Blake, J. E. Parker, C. C. Tang and M. Schröder, *Nature Chemistry* **2012**, *4*, 887–894.
5. C. E. Wilmer, O. K. Farha, T. Yildirim, I. Eryazici, V. Krungleviciute, A. A. Sarjeant, R. Q. Snurr, J. T. Hupp, *Energy Environ. Sci.* **2013**, *6*, 1158-1163; X.-J. Wang, P.-Z. Li, Y. Chen, Q. Zhang, H. Zhang, X. X. Chan, R. Ganguly, Y. Li, J. Jiang, Y. Zhao, *Sci. Rep.* **2013**, *3*, 12012
6. B. Zheng, Z. Yang, J. Bai, Y. Li, S. Li, *Chem. Commun.* **2012**, *48*, 7025-7027.
7. Z. Guo, H. Wu, G. Srinivas, Y. Zhou, S. Xiang, Z. Chen, Y. Yang, W. Zhou, M. O'Keeffe, B. Chen, *Angew. Chem. Int. Ed.* **2011**, *50*, 3178-3181.
8. I. Senkovska and S. Kaskel, *Micropor. Mesopor. Mat.* **2008**, *112*, 108-115.
9. H. Furukawa, N. Ko, Y. B. Go, N. Aratani, S. B. Choi, E. Choi, A. O. Yazaydin, R. Q. Snurr, M. O'Keeffe, J. Kim, O. M. Yaghi, *Science* **2010**, *329*, 424–428;
10. O. K. Farha, A. Özgür Yazaydın, I. Eryazici, C. D. Malliakas, B. G. Hauser, M. G. Kanatzidis, S. T. Nguyen, R. Q. Snurr, J. T. Hupp, *Nature Chemistry* **2010**, *2*, 944–948.
11. S. Ma, D. Sun, J. M. Simmons, C. D. Collier, D. Yuan, H.-C. Zhou, *J. Am. Chem. Soc.* **2008**, *130*, 1012-1016.
12. H. Wu, W. Zhou, T. Yildirim, *J. Am. Chem. Soc.* **2009**, *131*, 4995.-5000
13. C. E. Wilmer, M. Leaf, C. Y. Lee, O. K. Farha, B. G. Hauser, J. T. Hupp, R. Q. Snurr, *Nature Chem.* **2012**, *4*, 83-89.
14. D. Liu, H. Wu, S. Wang, Z. Xie, J. Li, W. Lin, *Chem. Sci.* **2012**, *3*, 3032-3037.
15. S. Bourrelly, P. L. Llewellyn, C. Serre, F. Millange, T. Loiseau, G. Férey, *J. Am. Chem. Soc.* **2005**, *127*, 13519-13521.
16. D. Yuan, D. Zhao, D. Sun, H.-C. Zhou, *Angew. Chem. Int. Ed.* **2010**, *49*, 5357-5361.
17. W. Zhou, H. Wu, M. R. Hartman, T. Yildirim, *J. Phys. Chem. C* **2007**, *111*, 16131-66137.